PERGAMON

Computers and Structures 67 (1998) 483–502

Computers & Structures

On control and optimization of elastic multilink mechanisms

Hsu-Lung Wang†, Jeffrey W Eischen*, Larry M Silverberg

Department of Mechanical and Aerospace Engineering, North Carolina State University, Raleigh, N.C. 27695, U.S.A.

Received 12 December 1996; received in revised form 8 December 1997

Abstract

This paper presents a simple method for control of nonlinear elastic multilink mechanisms. The associated control law consists of open and closed loop components. The open loop component produces the desired overall rigid body motion, while the closed loop component suppresses the elastic motion relative to rigid body motion. Both the control law and the structural dynamics are referred to an inertial coordinate system. As a consequence, the control forces and control moments are easily simulated in a dynamic finite element analysis program. A series of numerical simulations illustrate the generality of this new method.

1. Introduction

The simulation of elastic multilink systems is becoming an increasingly important tool in design. Typical examples of such systems include elastic linkages, high precision machine dynamics, robot manipulator arms, aircraft propellers, satellites with flexible appendages, and other types of deployable structures. The components of these structures typically undergo large relative displacements and rotations during operation.

There have been numerous investigations in the control of elastic mechanisms. Most existing control algorithms applied to elastic mechanisms assume that the system is linear. In fact, the equation governing the motion of elastic mechanisms undergoing large displacements and rotations is nonlinear. Moreover, most control algorithms are complicated and require some transfer matrices or knowledge of the modal quantities. Those considerations make the control implementation difficult, especially in more complicated mechanisms. The question arises as to whether it is possible to develop a strategy that uses simple control laws to control a nonlinear elastic mechanism effectively.

The primary objective of this paper is then to outline a simple, but effective, control strategy to manipulate multilink mechanisms undergoing large deformations. A finite element method, based on large displacement beam theory, is employed to simulate the kinematics and dynamics of elastic mechanisms.

A non-colocated large deflection control law was developed for a simple beam slewing problem [1]. A torque was applied at the beam root and sensor measurements were taken at the beam root and the beam tip. That paper proposed a strategy well suited for beams undergoing large elastic motions described by nonlinear partial differential equations of motion. The associated torque was governed by a slewing control algorithm consisting of open- and closed-loop components. The open-loop component produced the desired overall rigid body motion of the beam, while the closed-loop component suppressed the elastic vibrational motion relative to a shadow beam. The shadow beam is a fictitious beam whose motion is prescribed by the designer [2]. The shadow beam is essentially a straight line that remains tangent to the beam at its root. The closed loop control component was expressed as a function of three parameters: the colocation gain, the angular displacement gain, and

* Corresponding author.

† Current address: Institute of Biomedical Engineering, National Cheng Kung University, Tainen, Taiwan, People's Republic of China.

0045-7949/98/$19.00
PII: S0045-7949(98)00060-1

the angular rate gain. The angular displacement gain provides the beam with artificial stiffness, and the angular rate gain provides the beam with artificial damping for this class of structures [3]. This paper extends the previously described developments to more complicated mechanisms and a broader class of nonlinear control problems. We restrict our attention to direct feedback control to ensure system stability and the use of the shadow structure is no longer necessary with the new approach.

2. Large displacement beam theory

The kinematics and dynamics of elastic mechanisms can be described by large displacement beam theory with proper treatment of joint constraint conditions. The beam theory must allow arbitrarily large displacements and cross section rotations. The beam theory presented in this work is based on the concept proposed by Simo and Vu-Quoc [4] in which the motion is referred to an inertial frame. The resulting discretized equations of motion for large displacement beam theory are of the form commonly encountered in nonlinear structural dynamics, i.e.

$$\mathbf{Ma} + \mathbf{P(d)} = \mathbf{F(d, v)}, \tag{1}$$

where **d** stores nodal displacements and cross section rotations, **v** is nodal velocities and cross-section angular velocities ($\mathbf{v} = \dot{\mathbf{d}}$), and **a** stores nodal accelerations and cross-section angular accelerations ($\mathbf{a} = \ddot{\mathbf{d}}$). **M** is the symmetric system mass matrix. Note that the mass matrix is time invariant because kinematic quantities are referred to an inertial reference frame, i.e. there are no rotating frames. **P(d)** is the nonlinear internal force vector and **F(d,v)** is the system control force vector, which depends on certain nodal displacements (and rotations) and velocities (and angular velocities). Details regarding the numerical solution of Eq. (1) in which $\mathbf{F(d,v)} = \mathbf{F}(t)$ are given in the paper by Simo and Vu-Quoc. This computational procedure combines the Newton–Raphson method for solving systems of nonlinear algebraic equations with the Newmark method for solving second-order systems of ordinary differential equations.

3. Control law

The control force is the sum of an open loop control force and a closed loop control force,

$$\mathbf{F} = \mathbf{F}_o + \mathbf{F}_c, \tag{2}$$

where $\mathbf{F}_o$ is the open loop control force vector controlling rigid body motion and $\mathbf{F}_c$ is the closed loop control force vector controlling elastic motions relative to the rigid body motions.

3.1. Open-loop control

$\mathbf{F}_o$ are the forces necessary for the system to follow a specified desired path $\mathbf{d}_D$ at a desired rate $\dot{\mathbf{d}}_D$, assuming that the mechanism is rigid. The forces can be obtained either analytically or numerically. It is possible to derive the open loop forces analytically for simple mechanisms. However, for more complicated mechanisms, a numerical method is required. One of the numerical methods used in this work is the so called 'inverse dynamics' technique. Two FORTRAN codes, KAP and DAP, developed by Nikravesh [5] are used in rigid body kinematic and dynamic analyses. KAP, a program for solving planar kinematics of rigid body mechanisms, is used to determine unspecified nodal positions and velocities in terms of certain 'driving point' specified positions and velocities. DAP then iterates to solve for the required driving point forces and moments.

3.2. Closed loop control

Consider the linear time-invariant closed loop control force vector $\mathbf{F}_c$ controlling elastic motions relative to the rigid body motions,

$$\mathbf{F}_c = -\mathbf{G}(\mathbf{d} - \mathbf{d}_D) - \mathbf{H}(\dot{\mathbf{d}} - \dot{\mathbf{d}}_D), \tag{3}$$

where **d** and $\dot{\mathbf{d}}$ are the displacement vector and velocity vector, respectively, and $\mathbf{d}_D$ and $\dot{\mathbf{d}}_D$ are the desired displacement vector and velocity vector, respectively. **G** is the displacement control gain matrix, and **H** is the velocity control gain matrix. In general they are expressed as

$$\mathbf{G} = \begin{bmatrix} g_{11} & g_{12} & \cdots & g_{1n} \\ g_{21} & g_{22} & \cdots & g_{2n} \\ \vdots & \vdots & \ddots & \vdots \\ g_{n1} & g_{n2} & \cdots & g_{nn} \end{bmatrix} \quad \mathbf{H} = \begin{bmatrix} h_{11} & h_{12} & \cdots & h_{1n} \\ h_{21} & h_{22} & \cdots & h_{2n} \\ \vdots & \vdots & \ddots & \vdots \\ h_{n1} & h_{n2} & \cdots & h_{nn} \end{bmatrix} \tag{4}$$

where the displacement gain **G** provides the mechanism with artificial stiffness while the velocity gain **H** provides the mechanism with artificial damping.

3.3. Direct control

Direct control directly feeds back the sensor colocated with the actuator. Direct control is a special case of colocated control. All of the closed loop controls in our simulations are confined to direct control because the stability of a nonlinear system employing direct control can be guaranteed when the gains are

nonnegative. Furthermore, the stability can be characterized by examining the associated characteristic roots [3] or by examining the linearized feedback gain matrix [6]. The stability property was proven using an energy view point [7]. The displacement and velocity control gain matrices **G** and **H** in Eq. (4) are diagonal in direct control. We obtain

$$\mathbf{G}=\begin{bmatrix} g_{11} & 0 & \dots & 0 \\ 0 & g_{22} & \dots & 0 \\ \vdots & \vdots & \ddots & \vdots \\ 0 & \dots & \dots & g_{nn} \end{bmatrix} \mathbf{H}=\begin{bmatrix} h_{11} & 0 & \dots & 0 \\ 0 & h_{22} & \dots & 0 \\ \vdots & \vdots & \ddots & \vdots \\ 0 & \dots & \dots & h_{nn} \end{bmatrix}. \tag{5}$$

4. Performance function and optimization

4.1. Performance function

The design of a feedback control system for a complex mechanism is inherently an exercise in compromise. The compromises are mainly between the control effort and the dynamic performance [8]. A performance function is an objective function to be optimized or 'compromised'. It can be formulated by defining various kinds of functions depending on the demand and priority. We denote the performance function P by

$$P = P(x_1, x_2, x_3, \dots, x_n), \tag{6}$$

where the performance parameters x_i ($i = 1, 2, \dots, n$) are independent variables and can be characterized as one of three types. The first type are called control parameters, e.g. control gains, the location of the force actuators, and the measurement sensors. The second type are called physical parameters, e.g. mass, stiffness, and geometry. The third type are called dynamic parameters, e.g. natural/controlled modal frequencies and modal damping rates [3].

In elastic mechanism design, a common goal is to control the path of motion and to eliminate the vibration in a finite period (settling time) with the minimum fuel consumption. One candidate function is as follows,

$$P = \int_0^{\infty} \mathbf{F}_c^{\mathrm{T}}\mathbf{F}_c \, \mathrm{d}t + w\left(\int_0^{\infty} \mid E - E_{\mathrm{D}} \mid \mathrm{d}t\right) \tag{7}$$

where w is a positive weighting parameter and $\mathbf{F}_c$ is the closed loop control vector. $\mathbf{F}_c^{\mathrm{T}}\mathbf{F}_c$ represents the control power consumption, indicating the control effort. E is total energy; the sum of kinetic and strain energies. E_{D} is the desired energy (kinetic energy) assuming the mechanism is rigid. The term $E - E_{\mathrm{D}}$ is used to reflect residual vibration. Note that this performance function trades-off between power and energy depending on the weighting parameter w.

For implementation purposes, $\int_0^{\infty}$ is replaced by $\Sigma_{t=0}^{t=T_{\mathrm{f}}}$. Eq. (7) becomes

$$P = \sum_{t=0}^{t=T_{\mathrm{f}}} \mathbf{F}_c^{\mathrm{T}}\mathbf{F}_c \Delta t + w\left(\sum_{t=0}^{t=T_{\mathrm{f}}} \mid E - E_{\mathrm{D}} \mid \Delta t\right), \tag{8}$$

where T_{f} is an assigned finite time period, usually a large multiple of the maneuver time and long enough for vibration to be damped out. The performance function is calculated during each time step of the finite element simulation, and the results are accumulated as a sum, as indicated in the equation above. The performance function can also be modified as follows,

$$P = \sum_{t=T_{\mathrm{m}}}^{t=T_{\mathrm{f}}} \mathbf{F}_c^{\mathrm{T}}\mathbf{F}_c \Delta t + w\left(t\sum_{t=0}^{t=T_{\mathrm{f}}} E\Delta t\right). \tag{9}$$

This form emphasizes vibration suppression increasingly as time increases (after the open loop control force is released).

4.2. Optimization technique

The least-squares method is widely used in optimization procedures. In this paper, the Levenberg–Marquardt least squares method was adopted. This method takes advantage of reliable early convergence of the steepest descent method far from the optimum, while automatically switching to a rapidly convergent Newton–Raphson iteration as the minimum is approached [9]. If the performance function is quadratic, the global minimum can always be obtained.

4.3. Procedures

A systematic procedure for optimal control design of elastic mechanisms is outlined below along with a flow chart of procedures displayed in Fig. 1.

1. Modeling:
   (a) Define geometry, material properties and boundary conditions.
   (b) Determine the location and number of actuators and sensors.
   (c) Generate finite element mesh. It should be noted that the actuators and sensors must be located at the nodes of the mesh.
   (d) Specify desired positions and velocities (independent degrees of freedom).
2. Kinematics and inverse dynamics:
3. Treating the structure as rigid, solve for unspecified positions and velocities (dependent degrees of freedom) for the sensor locations. KAP is used in this stage.

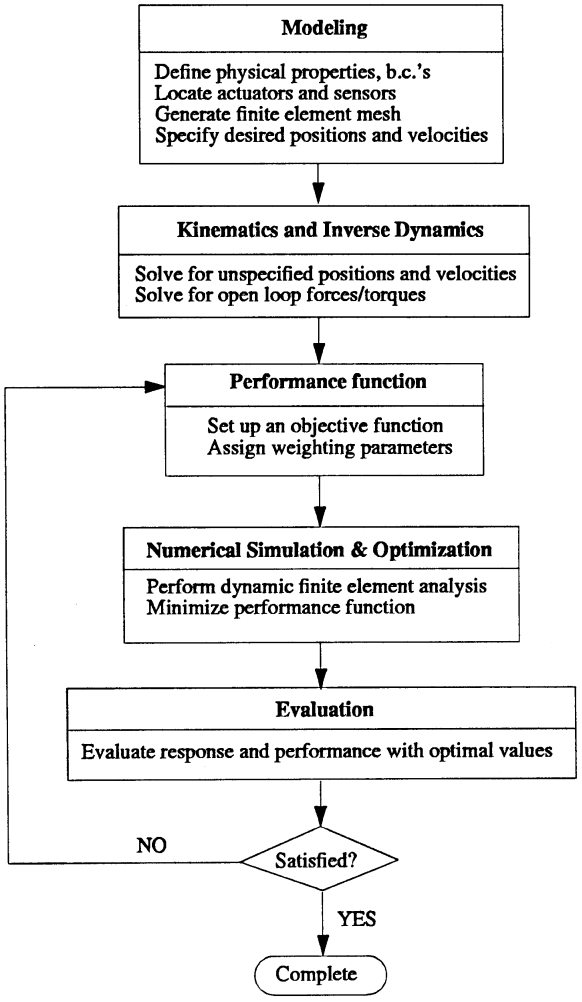

Fig. 1. Design procedure for optimal control of flexible mechanisms.

4. Solve for open loop forces/torques for the actuators. DAP is used in this stage.

Performance function and weighting parameters:

(a) Formulate an objective function to be minimized.
(b) Assign weighting parameters.

Simulation and optimization:

(a) Perform simulations using dynamic finite element analysis.
(b) Minimize the performance function and derive the performance parameters.

Evaluation: Evaluate all the performances or criteria, e.g. dynamic response and fuel consumptions, with the current optimal performance parameters. If they are satisfied then the design procedure is complete. If not, then go back to step 3, using new weighting parameters or using a new performance function.

5. Results

A series of numerical simulations are presented in this paper that illustrate the formulation and numerical procedures discussed in this paper. The trapezoidal rule (Newmark algorithm with $\gamma = 0.5$ and $\beta = 0.25$) was employed in the dynamic simulations. For all the mechanisms, the masses of the linkages and any payload other than concentrated masses are assumed to be uniformly distributed. Numerical operations were performed in double precision on an IBM RISC6000 system.

It is acknowledged that the following results are presented absent a formal stability proof. The fact that the underlying equations of motion are nonlinear and extremely complex due to the multibody feature for the class of problems being studied renders traditional stability analyses unfeasible—even Liapunov and other nonlinear stability analysis procedures. So in these situations, what is the control system designer to do? The approach, which is presented in this paper, relies on simulating the response. With respect to this, there are several simulation approaches, and the differences between them play a role in the control system design. In situations in which the actuation is continuous in time (like when motors are used) linear feedback can be quite adequate (including situations in which it is desirable to vary the gains) while in other situations in which the actuation is discrete in time (like when pneumatic devices are used) bang-off-bang approaches are appropriate. In still other situations different types of actuation are required to work together. Furthermore, the associated cost functions are not necessarily of the classical forms, e.g. LQR and minimum time/fuel. This paper addresses many of these situations. There are certainly many papers in the literature that deal primarily with algorithm development and not complex nonlinear response.

Indeed, this paper presents a reasonably general approach to designing feedback control systems for these types of complex mechanisms. The generality allows for a wide family of cost functions, and the structure is allowed to exhibit nonlinear behavior.

5.1. Slewing beam

5.1.1. Numerical modeling

This simulation manipulates the flexible hinged-free beam shown in Fig. 2. An open loop and closed loop torque are applied at the beam root in order to achieve a 90° rest-to-rest maneuver, while minimizing residual

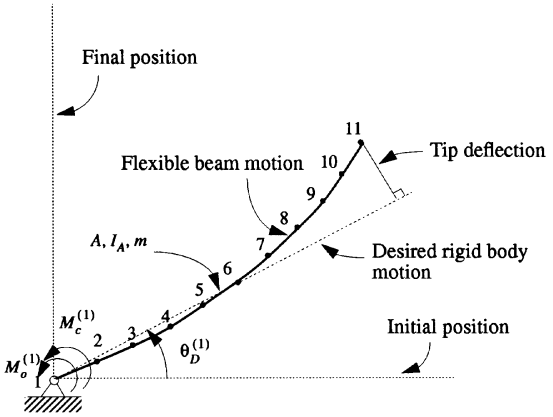

Fig. 2. Slewing beam.

vibration. The finite element mesh consists of 10 elements with linear isoparametric interpolation functions for both displacement and rotation. A time step size $\Delta t = 0.005$ s was used in performing the dynamic finite element analysis. The physical properties are listed in Table 1.

5.1.2. Open-loop control

The desired root angle $\theta_D^{(1)}$ is expressed in polynomial form: $\theta_D^{(1)}(t) = a_0 + a_1 t + a_2 t^2 + a_3 t^3 + a_4 t^4 + a_5 t^5$ ($t \leqslant T_m$), where T_m is the desired maneuver time. The coefficients a_0 through a_5 are determined by appropriate initial and final maneuver states. For instance, in the numerical example presented here, the beam is slewed 90° counterclockwise in a rest-to-rest maneuver. The initial and final states are: $\theta_D^{(1)}(0) = 0$, $\dot{\theta}_D^{(1)}(0) = 0$, $\ddot{\theta}_D^{(1)}(0) = 0$, $\theta_D^{(1)}(T_m) = \pi/2$, $\dot{\theta}_D^{(1)}(T_m) = 0$, and $\ddot{\theta}_D^{(1)}(T_m) = 0$. For $T_m = 2$ s the desired root angle response is obtained as shown in Fig. 3, i.e. $\theta_D(t) = 1.9634954t^3 - 1.4726216t^4 + 0.2945243t^5 (t < 2.0)$ and $\theta_D(t) = \pi/2 (t \geqslant 2.0)$. The open-loop torque M_0 is defined as the torque required to maneuver the beam along the desired path if it were rigid. Thus, according to rigid body dynamics, the open loop control torque that would be applied at the root of the equivalent rigid beam is expressed as $M_0^{(1)}(t) = I_L \ddot{\theta}_D^{(1)}(t)$, where $I_L = mL^2/3$ is the mass moment of inertia of the rigid beam about the hinge point and m is the total mass of the beam and payload. The required open loop torque is shown in Fig. 4.

Table 1
Physical parameters for the slewing beam

Physical parameters	
Length (cm)	$L = 100$
Cross-section area (cm^2)	$A = 0.1$
2nd moment of area (cm^4)	$I_A = 8.333 \times 10^{-5}$
Total mass of linkage and payload (g)	$m = 120.0$
Elastic modulus (kPa)	$E = 6.895 \times 10^7$
Shear modulus (kPa)	$G = 2.758 \times 10^7$

To increase the flexibility and to lower the fundamental frequency, a payload has been added on the linkages in the simulations. Fig. 5 shows the oscillatory response at the tip as a function of the combined mass

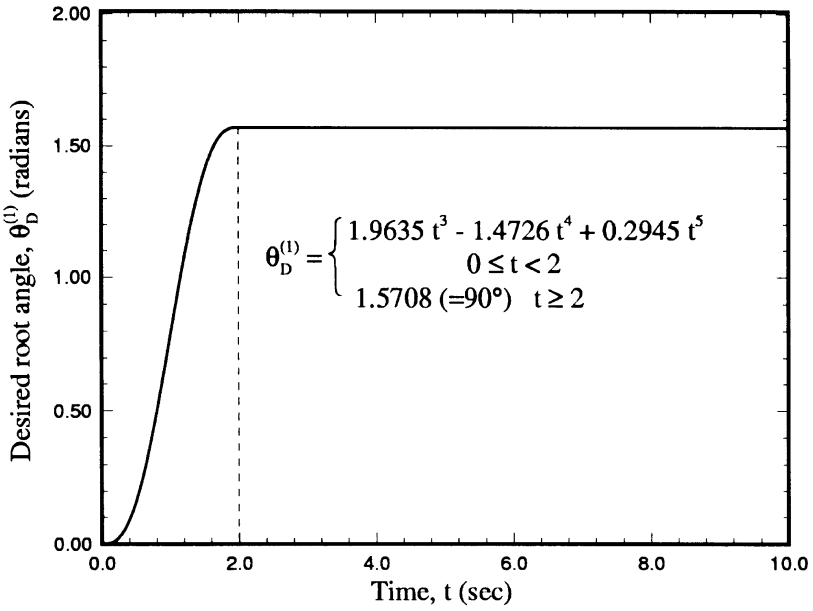

Fig. 3. Desired angle for the slewing beam.

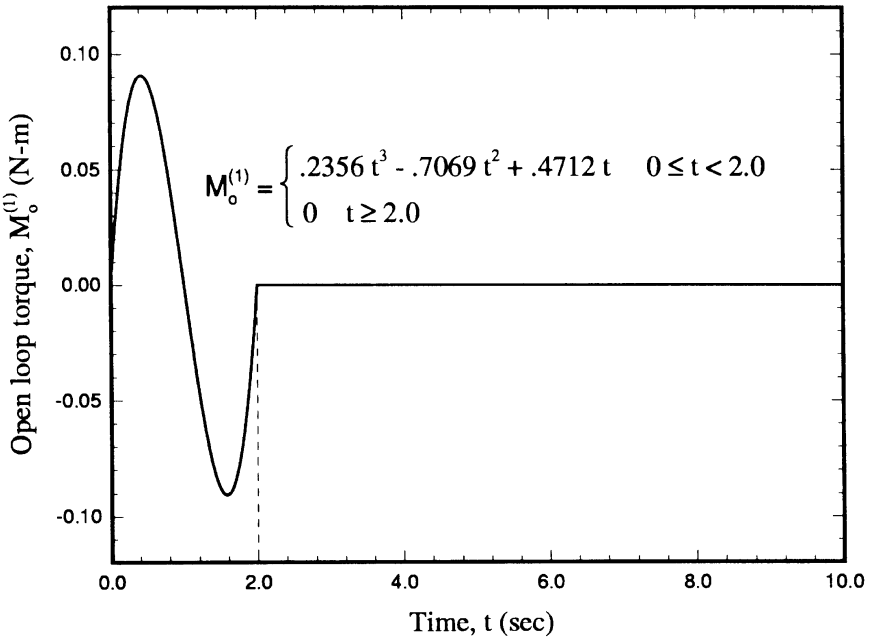

Fig. 4. Open-loop torque for the slewing beam.

per unit length of the beam and added payload. The parameter used to show this effect is $\rho_T = m/L$. The amplitude of the deflection of the beam is dominated by the first natural mode of vibration of the beam (bending). Fig. 6 shows an energy partition for three values of ρ_T. Note that the total energy (strain energy + kinetic energy) remains constant for $t \geqslant T_m$, i.e. after the maneuver is completed. Based on this evaluation, $\rho_T = 1.2$ g/cm was chosen for the simulation given in the next section.

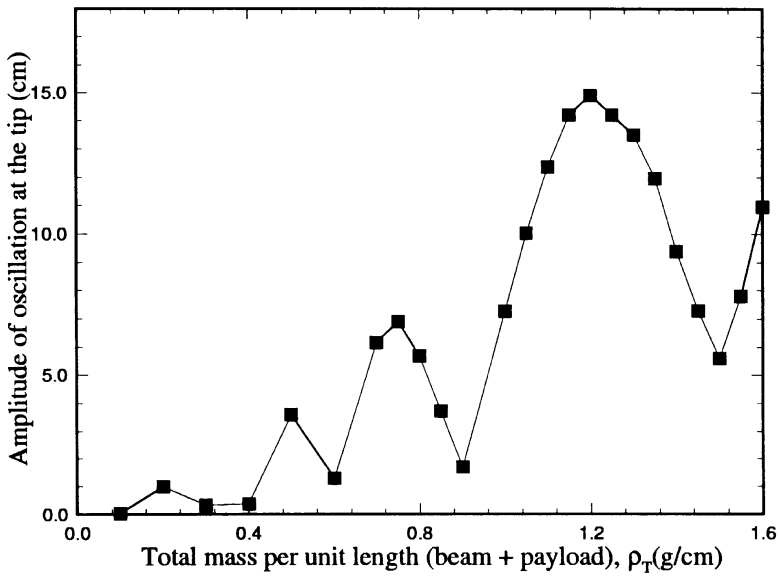

Fig. 5. The amplitude of oscillation at the tip for various combined mass per unit length of the beam and added payload ρ_T.

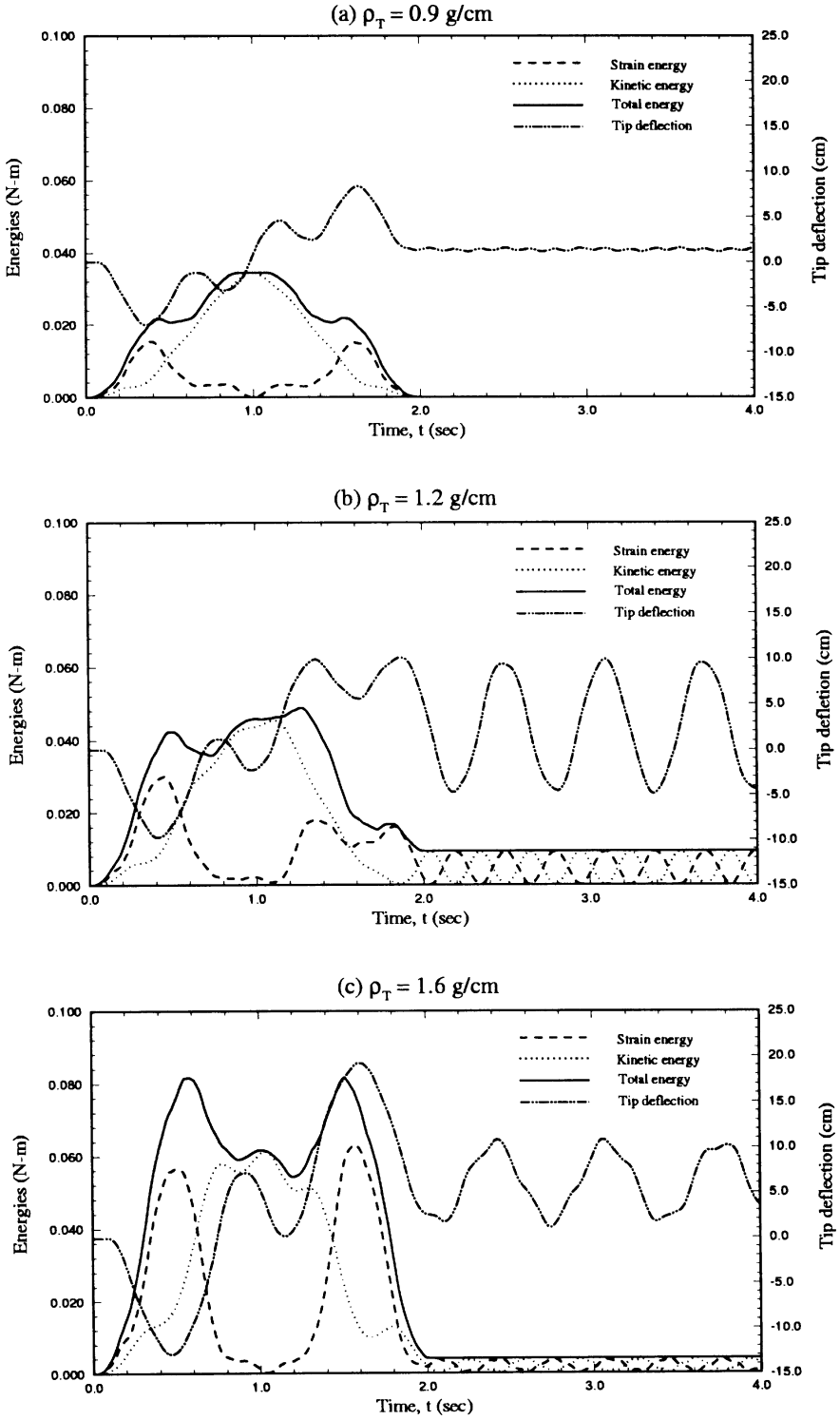

Fig. 6. The energies and tip deflection with (a) $\rho_T = 0.9$ g/cm (b) $\rho_T = 1.2$ g/cm (c) $\rho_T = 1.6$ g/cm.

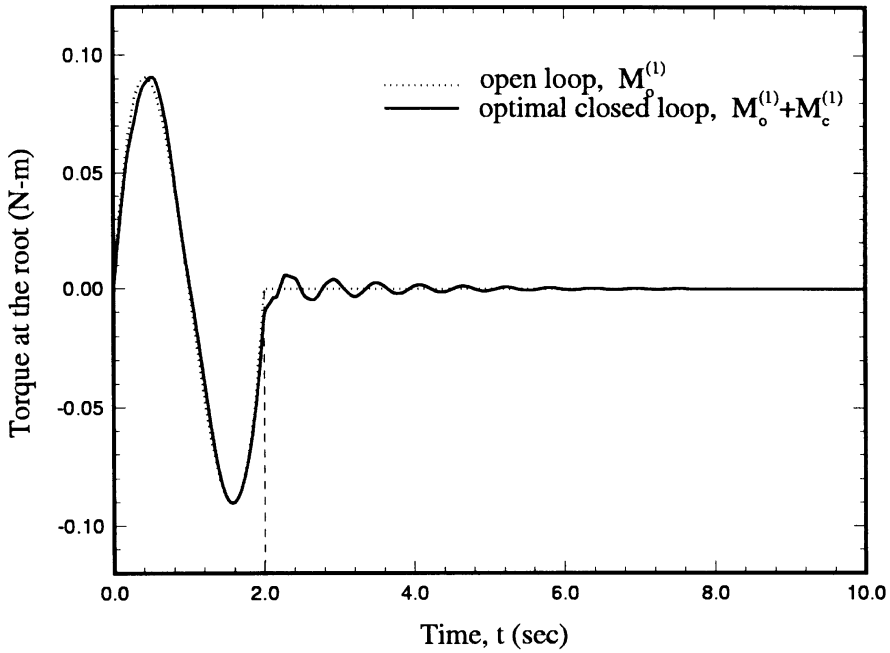

Fig. 7. The optimal applied torque $M_o^{(1)}+M_c^{(1)}$ ($g_1=0.0420$, $h_1=0.1463$).

5.1.3. Closed-loop control

The closed loop control law is defined as,

$$M_c^{(1)}=\begin{cases}-g_1 I_L(\theta^{(1)}-\theta_D^{(1)})-h_1 I_L(\dot\theta^{(1)}-\dot\theta_D^{(1)}) & 0<t\le T_m\\ -g_1 I_L[\theta^{(1)}-\theta_D^{(1)}(T_m)]-h_1 I_L\dot\theta^{(1)} & t\ge T_m\end{cases}, \tag{10}$$

where g_1 and h_1 are the displacement and velocity control gains, respectively, and where $\theta^{(1)}$ and $\dot\theta^{(1)}$ are the root angle and angular velocity, respectively.

The performance function is chosen as

$$P=\sum_{t=0}^{t=T_f} M_c^2\Delta t + w\left(t\sum_{t=0}^{t=T_f}\mid E-E_D\mid \Delta t\right), \tag{11}$$

where $M_c=M_c^{(1)}$ and $T_f=10$ s. The performance func-

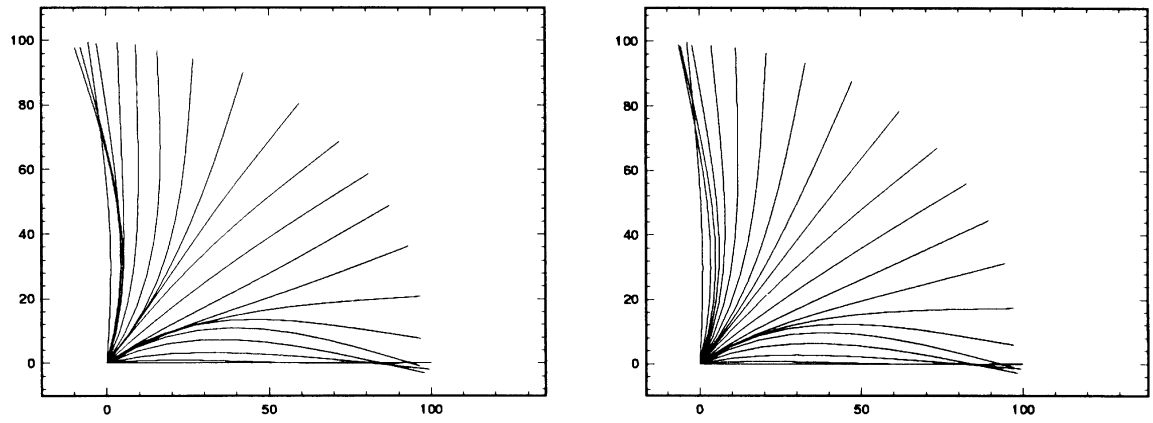

Fig. 8. Time-lapse responses of a single beam slewing (0–2 s) with time increment 0.1 s. Comparison between open-loop and optimal closed-loop responses ($g_1=0.0420$, $h_1=0.1463$).

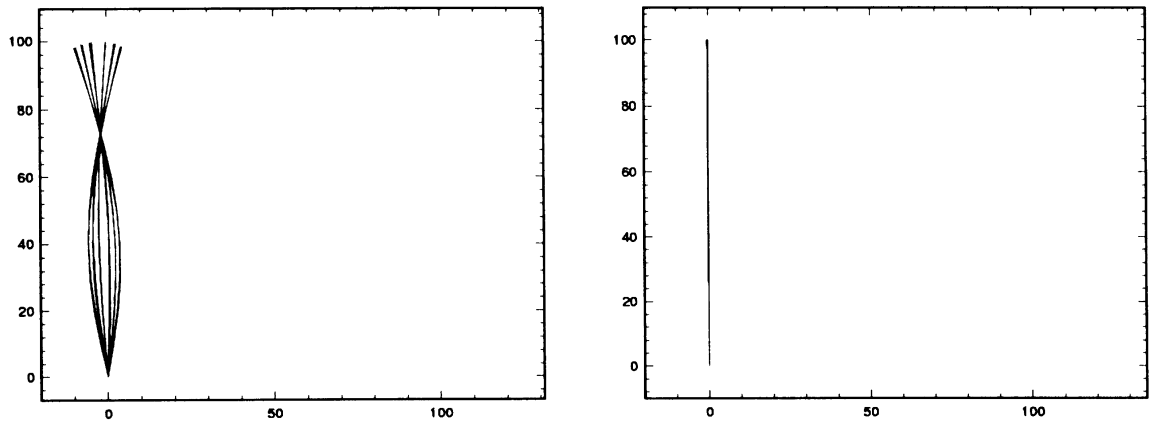

Fig. 9. Time-lapse responses of a beam slewing (8–10 s) with time increment 0.1 s. Comparison between open-loop and optimal closed-loop responses ($g_1 = 0.0420$, $h_1 = 0.1463$).

tion P is minimized after selecting a weighting parameter $w = 5.0 \times 10^4$(g cm^2/s).

The optimal torque ($g_1 = 0.0420\ s^{-2}$, $h_1 = 0.1463\ s^{-1}$) is shown in Fig. 7. The associated deflection is shown in Fig. 8 (0–2 s) and Fig. 9 (8–10 s). A family of optimal solutions was obtained by varying the weighting parameter in the performance function as shown in Fig. 10. As expected, the weighting parameter w increases with the control effort needed to reduce the energy in the system.

5.2. Crank-slider mechanism

5.2.1. Numerical modeling

This simulation manipulates the flexible crank-slider mechanism shown in Fig. 11. An open loop torque is applied at the root of the crank while a horizontal closed-loop feedback force is employed at the slider. The finite element mesh consists of five elements per link. A time step size of $\Delta t = 0.02$ s was used and the physical properties are listed in Table 2.

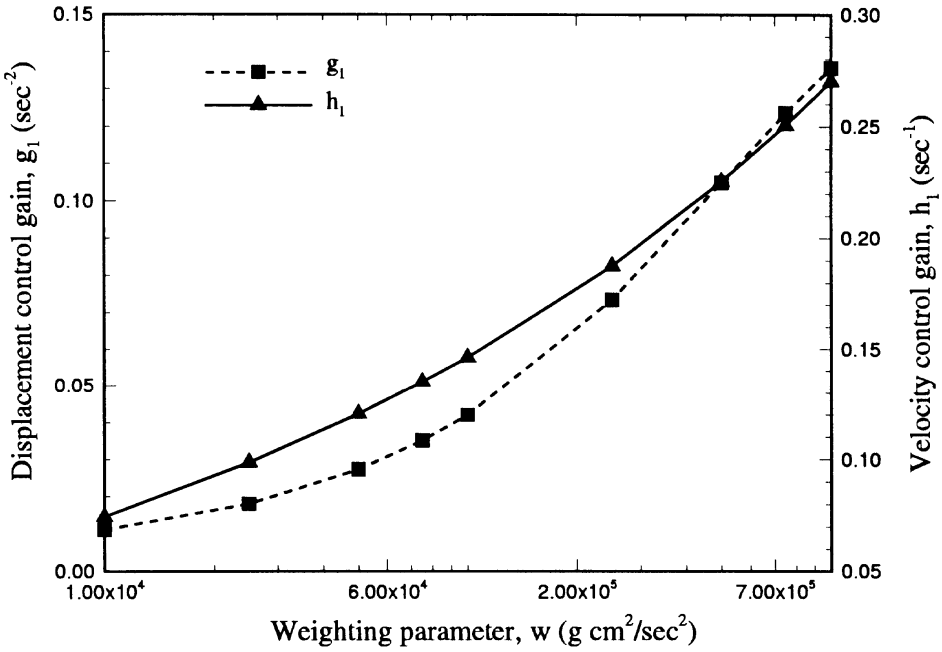

Fig. 10. Optimal control gains, g_1 and h_1, vs the weighting parameter w.

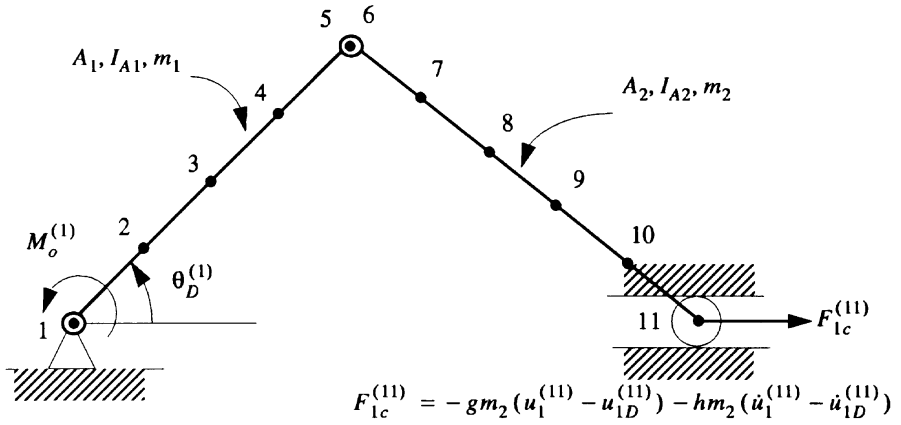

Fig. 11. Crank-slider mechanism with an open-loop control torque at the root and a closed-loop control force at the slider.

5.2.2. Open-loop control

Assume the crank is driven 90° counterclockwise in a rest-to-rest maneuver in 2 s. The desired crank angle $\theta_D^{(1)} = 1.9634954t^3 - 1.4726216t^4 + 0.2945243t^5 \quad (t < 2.0)$ and $\theta_D^{(1)} = 1.5707963$ $(t \geqslant 2.0)$ as shown in Fig. 12. The open loop torque M_o is defined as the torque to maneuver the crank-slider mechanism along the desired path assuming both links are rigid. This torque was determined using inverse dynamics and is shown in Fig. 13.

5.2.3. Closed-loop control

To control the vibration of the slider, a horizontal feedback control force was applied at that point (node 11) as shown in Fig. 11. This closed loop control force $F_{1c}^{(11)}$ is defined as

$$F_{1c}^{(11)} = \begin{cases} -g_1 m_2(u_1^{(11)} - u_{1D}^{(11)}) - h_1 m_2(\dot{u}_1^{(11)} - \dot{u}_{1D}^{(11)}) & 0 \leq t < T_m \\ -g_1 m_2(u_1^{(11)} - u_{1D}^{(11)}(T_m)) - h_1 m_2 \dot{u}_1^{(11)} & t \geq T_m \end{cases} \tag{12}$$

where m_2 is the total mass of the follower link. The time dependent slider displacement and velocity are denoted by $u_1^{(11)}$ and $\dot{u}_1^{(11)}$, respectively; while the desired slider displacement and velocity are $u_{1D}^{(11)}$ and $\dot{u}_{1D}^{(11)}$, respectively.

The performance function is chosen as

$$P = \sum_{t=0}^{t=T_f} (F_{1c}^{(11)})^2 \Delta t + w\left(t \sum_{t=0}^{t=T_f} | E - E_D | \Delta t\right), \tag{13}$$

where $T_f = 10$ s. The performance function P is minimized after selecting a weighting parameter $w = 5.0 \times 10^4$ (g cm^2/s). The open-loop and optimal closed-loop control system responses are displayed in Fig. 14 (0–2 s) and Fig. 15 (8–10 s). The slider vibration is suppressed very well in the finite time. However, due to a lack of damping in the open loop system, the mechanism 'freely drifts' after the open loop torque is removed. As shown, the closed loop control eliminates the drift.

5.3. Four-bar mechanism

5.3.1. Numerical modeling

This simulation manipulates the flexible four-bar mechanism shown in Fig. 16. An open loop torque is applied at the root of crank, while horizontal and vertical closed loop control forces are applied at node 12; a node between the coupler and the follower. The finite element mesh consists of four elements in the crank,

Table 2
Physical parameters for the crank-slider mechanism

Physical parameters	Crank	Slider
Length (cm)	$L_1 = 80$	$L_2 = 100$
Cross-section area (cm^2)	$A_1 = 0.5$	$A_2 = 0.5$
2nd moment of area (cm^4)	$I_{A1} = 0.01$	$I_{A2} = 0.01$
Total mass of linkage and payload (kg)	$m_1 = 16$	$m_2 = 2$
Elastic modulus (kPa)	$E = 6.895 \times 10^7$	
Shear modulus (kPa)	$G = 2.758 \times 10^7$	
Distance between ground pivots (cm)	180 (at $t = 0$ s)	

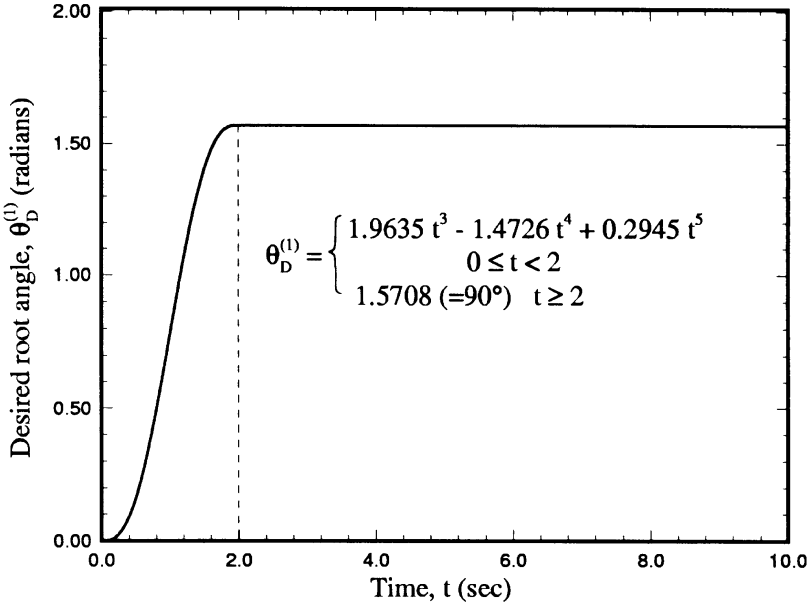

Fig. 12. Desired hinge angle for the crank-slider mechanism.

six elements in the coupler, and six elements in the follower. A time step size of $\Delta t = 0.0025$ s was used and the physical properties are listed in Table 3.

5.3.2. Open-loop control

The crank is driven counterclockwise in a rest-to-rest maneuver. For the maneuver time $T_m = 1$ s, the desired crank angle is $\theta_D^{(1)} = 9.272952t^3 - 13.909428t^4 + 5.563771t^5$ $(t < 1.0)$ and $\theta_D^{(1)} = 0.927295$ $(t \geqslant 1.0)$ as shown in Fig. 17. The open-loop torque $M_o^{(1)}$ is defined as the torque to maneuver the four-bar mechanism along the desired path assuming all three links are rigid as shown in Fig. 18. The open-loop torque was derived by the inverse dynamics method.

5.3.3. Closed-loop control

To control the vibration at the joint between the coupler and follower (node 12), horizontal and vertical

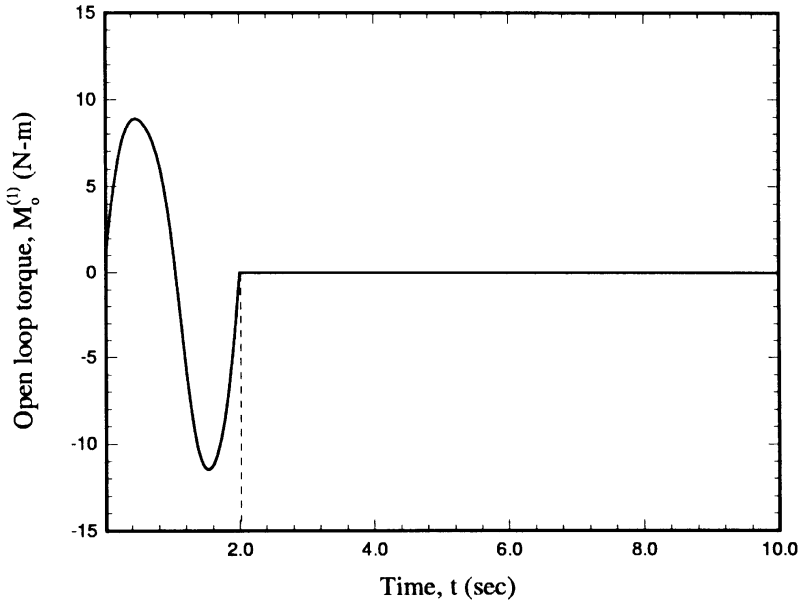

Fig. 13. Open loop hinge torque for the crank-slider mechanism.

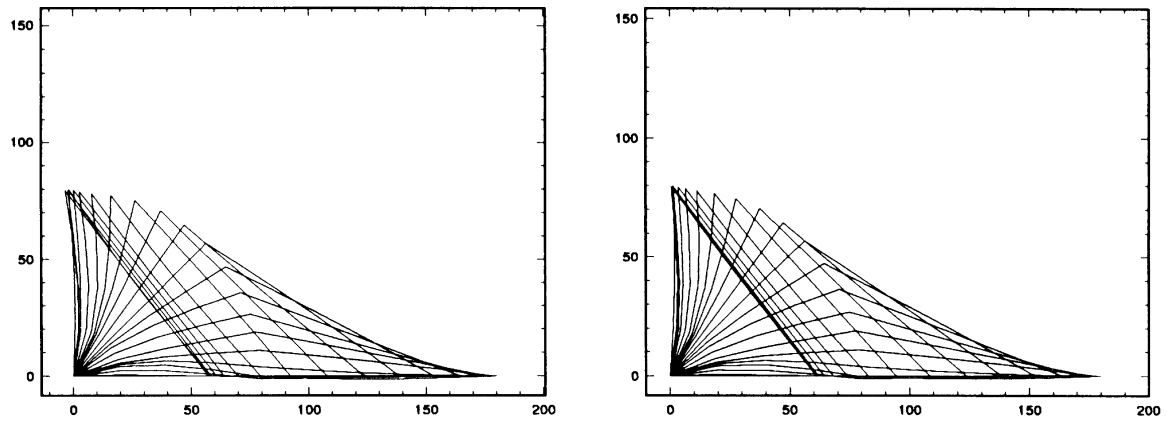

Fig. 14. Time-lapse responses of a crank-slider mechanism (0–2 s) with time increment 0.1 s. Comparison between open-loop and optimal closed-loop responses ($g_1 = 7.91$, $h_1 = 18.81$).

feedback control forces are applied at this node as shown in Fig. 16. The closed loop control forces, $F_{1c}^{(12)}$ and $F_{2c}^{(12)}$, are defined as

$$F_{1c}^{(12)} = \begin{cases} -g_1 m_3 (u_1^{(12)} - u_{1D}^{(12)}) - h_1 m_3 (\dot{u}_1^{(12)} - \dot{u}_{1D}^{(12)}) & 0 \le t < T_m \\ -g_1 m_3 [u_1^{(12)} - u_{1D}^{(12)}(T_m)] - h_1 m_3 \dot{u}_1^{(12)} & t \ge T_m \end{cases} \tag{14}$$

$$F_{2c}^{(12)} = \begin{cases} -g_2 m_3 (u_2^{(12)} - u_{2D}^{(12)}) - h_2 m_3 (\dot{u}_2^{(12)} - \dot{u}_{2D}^{(12)}) & 0 \le t < T_m \\ -g_2 m_3 (u_2^{(12)} - u_{2D}^{(12)}(T_m)) - h_2 m_3 \dot{u}_2^{(12)} & t \ge T_m \end{cases}, \tag{15}$$

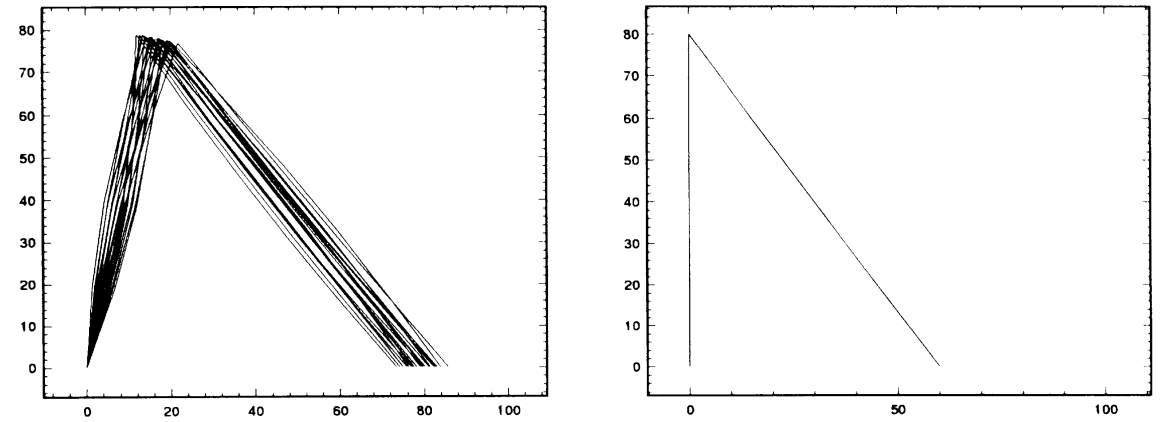

Fig. 15. Time-lapse responses of a crank-slider mechanism (8–10 s) with time increment 0.1 s. Comparison between open-loop and optimal closed-loop responses ($g_1 = 7.91$, $h_1 = 18.81$).

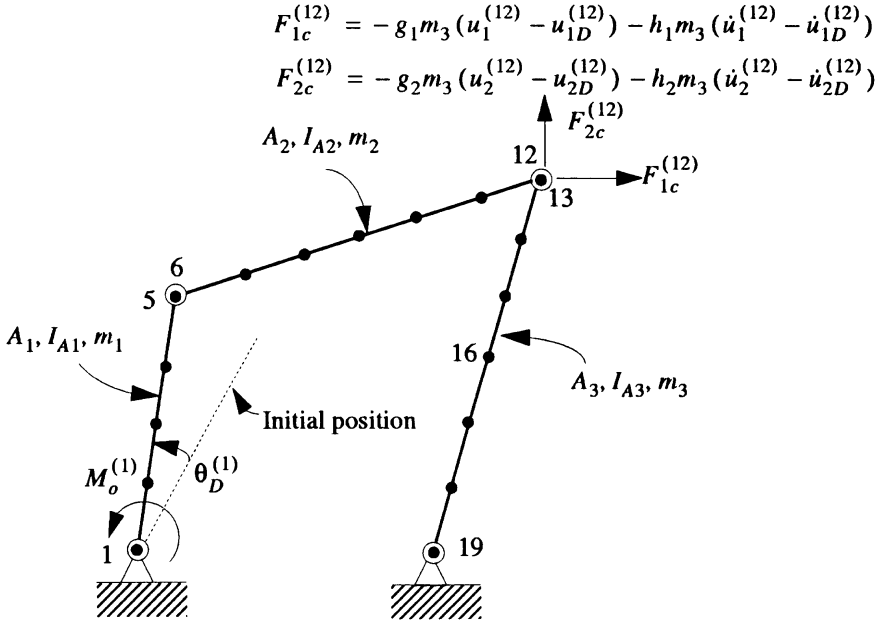

Fig. 16. Four-bar mechanism with an open-loop control torque at node 1 and two closed-loop control forces at node 12.

where m_3 is the total mass of the follower. It is noted that m_3 can be replaced by the mass of the coupler m_2 in above equations. The choice of either m_2 or m_3 is insignificant. The control forces can be expressed in matrix form [corresponding to Eq. (3)] as follows:

$$\mathbf{F}_c = [F_{1c}^{(12)} F_{2c}^{(12)}]^T, \quad \mathbf{d} = [u_1^{(12)} u_2^{(12)}]^T, \quad \dot{\mathbf{d}} = [\dot{u}_1^{(12)} \dot{u}_2^{(12)}]^T,$$
$$\mathbf{d}_D = [u_{1D}^{(12)} u_{2D}^{(12)}]^T, \quad \dot{\mathbf{d}}_D = [\dot{u}_{1D}^{(12)} \dot{u}_{2D}^{(12)}]^T,$$

and

$$\mathbf{G} = m_3 \begin{bmatrix} g_1 & 0 \\ 0 & g_2 \end{bmatrix} \quad \mathbf{H} = m_3 \begin{bmatrix} h_1 & 0 \\ 0 & h_2 \end{bmatrix}.$$

The performance function is chosen as

$$P = \sum_{t=0}^{t=T_f} \mathbf{F}_c^T \mathbf{F}_c \Delta t + w \left(t \sum_{t=0}^{t=T_f} | E - E_D | \Delta t \right), \tag{16}$$

where $T_f = 5$ s. The performance function P is minimized after selecting a weighting parameter $w = 3.0 \times 10^4$ (g cm^2/s). The optimal control gains are then obtained using the optimization. The open loop and optimal closed loop control responses are shown in Fig. 19 (0–2 s) and Fig. 20 (8–10 s). These figures show the reduction in the vibration of each of link using the closed loop control.

Fig. 21 shows the optimal control gains versus the weighting parameters. It is noted that there is a drop-off in velocity control gain h_2 when $w \geqslant 5 \times 10^4$. Usually when the weighting parameter w increases, indicating more emphasis in total energy (or vibration suppression), the control gains increase accordingly. However, when one of the control gains reaches its critical value, an overdamping occurs in the system. It follows that this control gain will decrease as w further increases. In this example, h_2 reaches the critical value when w is near 5×10^4.

Table 3
Physical parameters for the four-bar mechanism

Physical parameters	Crank	Coupler	Follower
Length (cm)	$L_1 = 44.72$	$L_2 = 63.25$	$L_3 = 67.08$
Cross-section area (cm^2)	$A_1 = 0.3$	$A_2 = 0.2$	$A_3 = 0.1$
2nd moment of area (cm$^4 \times 10^{-4}$)	$I_{A1} = 22.5$	$I_{A2} = 6.667$	$I_{A3} = 8.333$
Total mass of linkage and payload (kg)	$m_1 = 3.602$	$m_2 = 0.6794$	$m_3 = 0.3602$
Elastic modulus (kPa)	$E = 6.895 \times 10^7$		
Shear modulus (kPa)	$G = 2.758 \times 10^7$		
Distance between ground pivots (cm)	100		

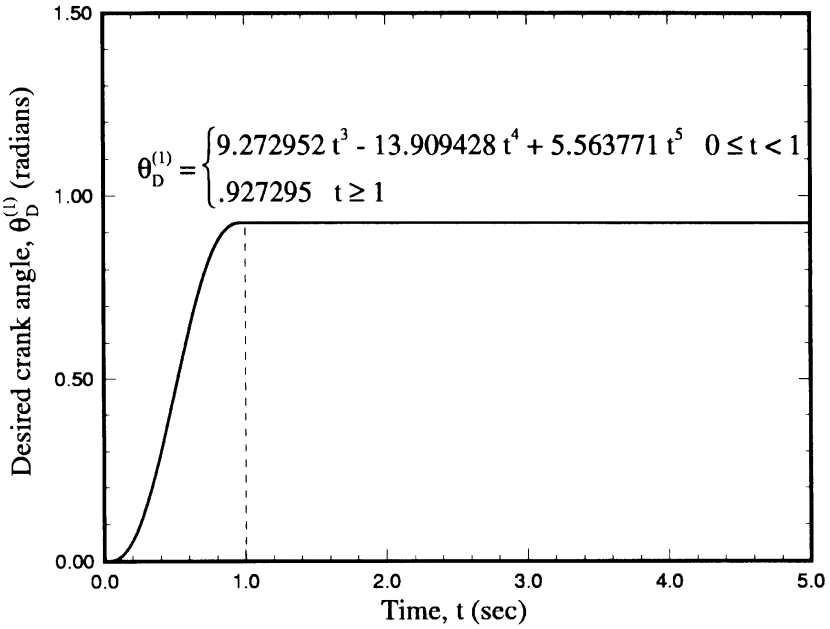

Fig. 17. Desired crank angle for the four-bar mechanism.

5.4. Two-arm robot

5.4.1. Numerical modeling

This simulation manipulates the planar two-arm robot with two revolute joints shown in Fig. 22. Open- and closed-loop control torques are applied to arm 1 while coupled internal open- and closed-loop control torques are applied at the joint between arms 1 and 2. The finite element mesh consists of four elements per arm. A time step size $\Delta t = 0.0025$ s was used and the physical properties are listed in Table 4.

5.4.2. Open-loop control

Assume both arms 1 and 2 (relative to arm 1) are driven 90° counterclockwise in a rest-to-rest maneuver. The maneuver time is $T_m = 2$ s, the crank angle θ_1 is $\theta_1^{(1)} = 1.9634954t^3 - 1.4726216t^4 + 0.2945243t^5 \quad (t \leqslant 2.0)$ and $\theta_1^{(1)} = 1.5707963 \quad (t > 2.0)$ as shown in Fig. 23. The

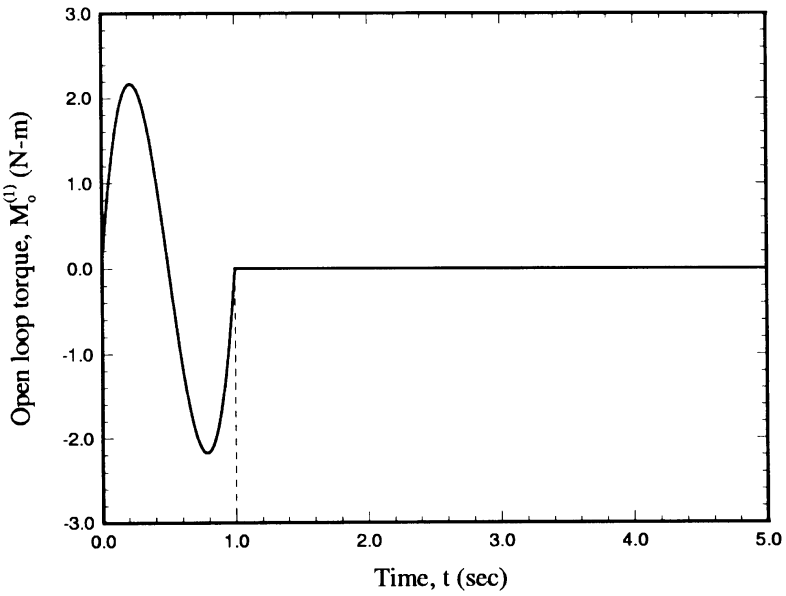

Fig. 18. Open-loop torque applied to the crank.

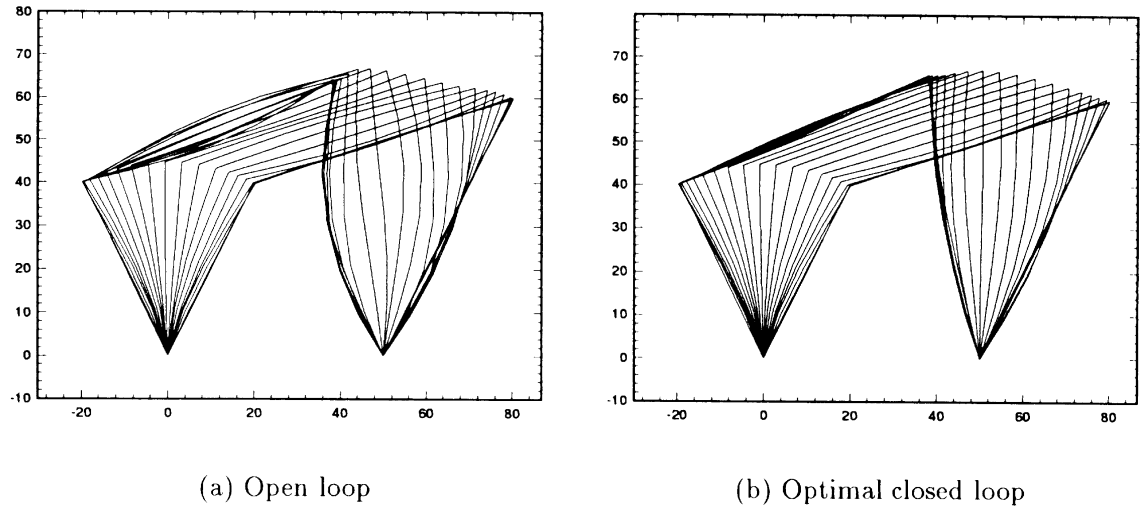

Fig. 19. Time-lapse responses of a four-bar mechanism (0–2 s) with time increment 0.1 s. Comparison between open-loop and optimal closed-loop responses ($g_1 = 112$, $h_1 = 32.5$, $g_2 = 317$, $h_2 = 54.6$).

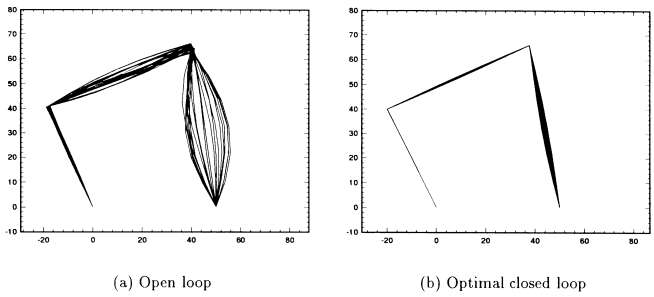

Fig. 20. Time-lapse responses of a four-bar mechanism (8–10 s) with time increment 0.1 s. Comparison between open-loop and optimal closed-loop responses ($g_1 = 112$, $h_1 = 32.5$, $g_2 = 317$, $h_2 = 54.6$).

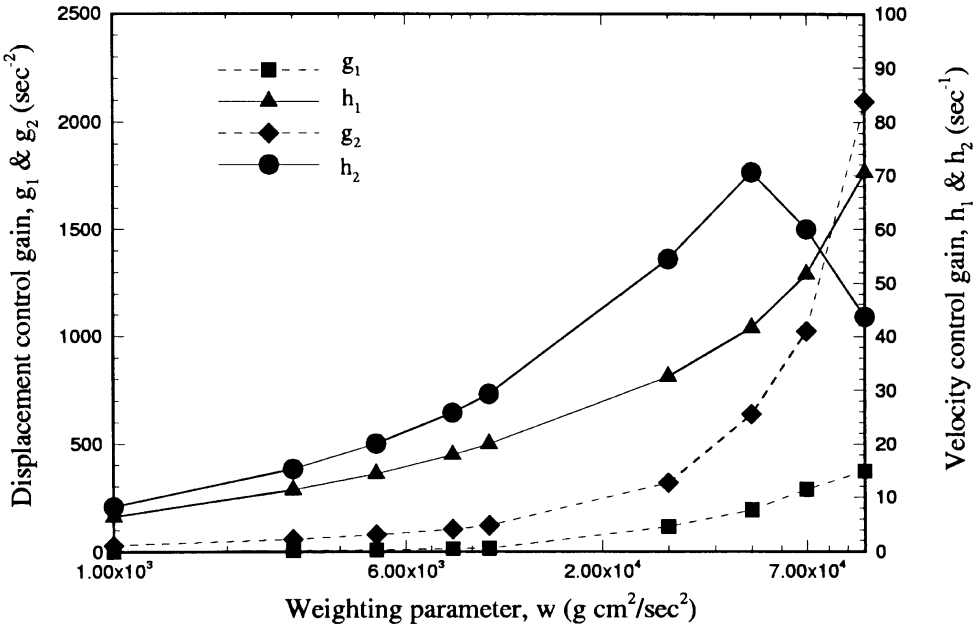

Fig. 21. Optimal control gains, g_1, h_1, g_2 and h_2, vs the weighting parameter.

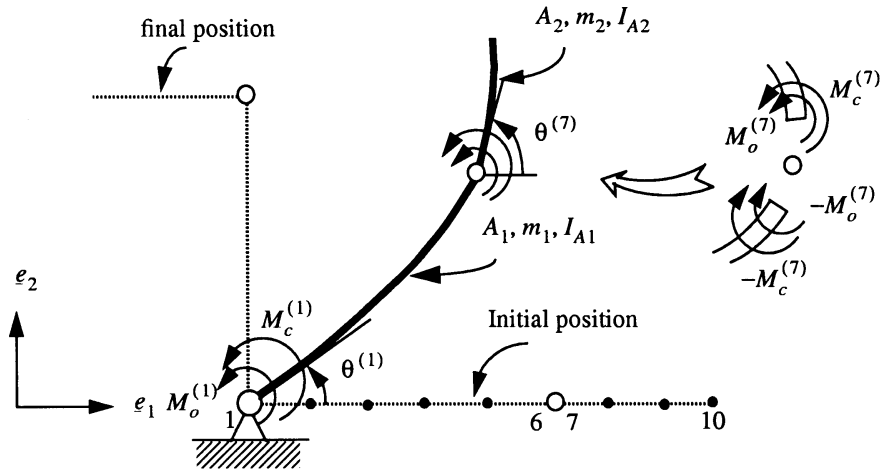

Fig. 22. Closed-loop control for the two-arm robot.

open-loop torques $M_o^{(1)}$ and $M_o^{(7)}$ $(= -M_o^{(6)})$ are defined as the torques required to manipulate arms 1 and 2, assuming that the two arms are rigid, as shown in Fig. 24.

5.4.3. Closed-loop control

To control the vibration of the arm angles $\theta^{(1)}$ and $\theta^{(7)}$, a closed loop torque $M_c^{(1)}$ and a pair of internal torques $M_c^{(6)}$ and $M_c^{(7)}$, are applied at nodes 1 and 6, respectively, as shown in Fig. 22. The closed loop control torques, $M_c^{(1)}$, $M_c^{(6)}$ and $M_c^{(7)}$ are defined as

$$M_c^{(1)} = \begin{cases} -g_1 I_{L1}(\theta^{(1)} - \theta_D^{(1)}) - h_1 I_{L1}(\dot{\theta}^{(1)} - \dot{\theta}_D^{(1)}) & 0 \le t \le T_m \\ -g_1 I_{L1}[\theta^{(1)} - \theta_D^{(1)}(T_m)] - h_1 I_{L1}\dot{\theta}^{(1)} & t \ge T_m \end{cases} \tag{17}$$

$$M_c^{(7)} = \begin{cases} -g_2 I_{L2}(\theta^{(7)} - \theta_D^{(7)}) - h_2 I_{L2}(\dot{\theta}^{(7)} - \dot{\theta}_D^{(7)}) & 0 \le t \le T_m \\ -g_2 I_{L2}[\theta^{(2)} - \theta_D^{(2)}(T_m)] - h_2 I_{L2}\dot{\theta}^{(7)} & t \ge T_m \end{cases} \tag{18}$$

$$M_C^{(6)} = -M_c^{(7)}, \tag{19}$$

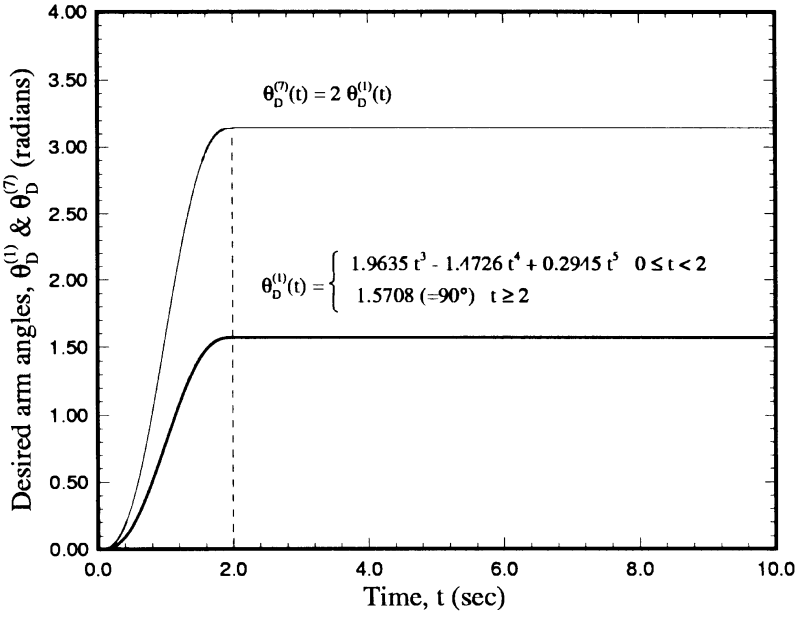

Fig. 23. Desired angle of $\theta_D^{(1)}$ and $\theta_D^{(7)}$ for the two-arm robot.

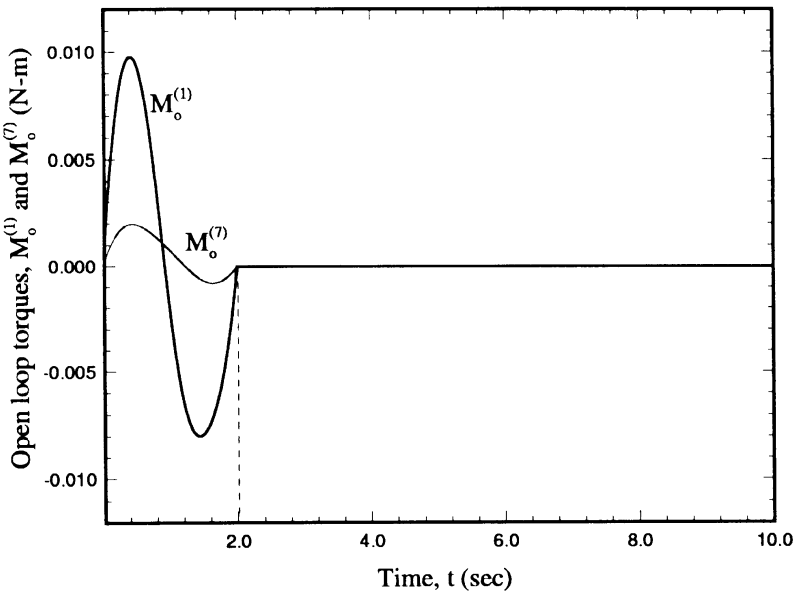

Fig. 24. Two open-loop torques, $M_o^{(1)}$ and $M_o^{(7)}$, applied at the root of arms 1 and 2, respectively.

Table 4
Physical parameters for the two-arm robot

Physical parameters	Arm 1	Arm 2
Length (cm)	$L_1 = 100$	$L_2 = 60$
Cross-section area (cm^2)	$A_1 = 0.01$	$A_2 = 0.01$
2nd moment of area ($cm^4 \times 10^{-6}$)	$I_{A1} = 8.3333$	$I_{A2} = 8.3333$
Total mass of linkage (kg)	$m_1 = 0.2685$	$m_2 = 0.1611$
Elastic modulus (kPa)	$E = 6.895 \times 10^7$	
Shear modulus (kPa)	$G = 2.758 \times 10^7$	

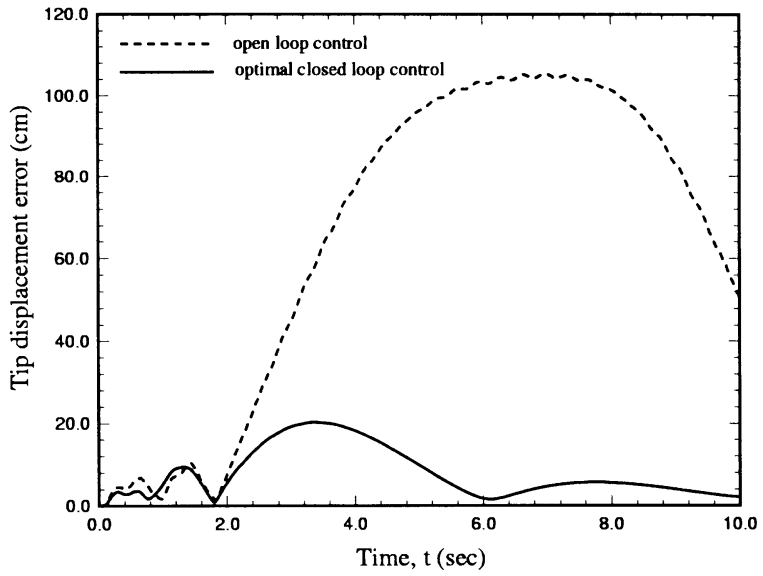

Fig. 25. Comparison between open-loop and optimal closed-loop ($g_1 = 3.43$, $h_1 = 2.42$, $g_2 = 0.88$, $h_2 = 1.13$) tip displacement errors.

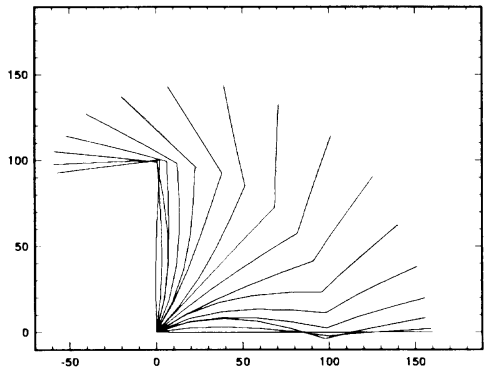

(a) 0 sec - 2 sec

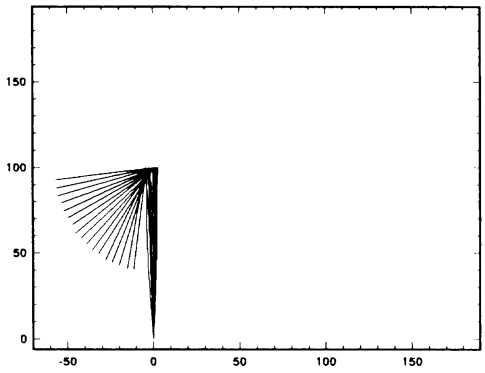

(b) 2 sec - 4 sec

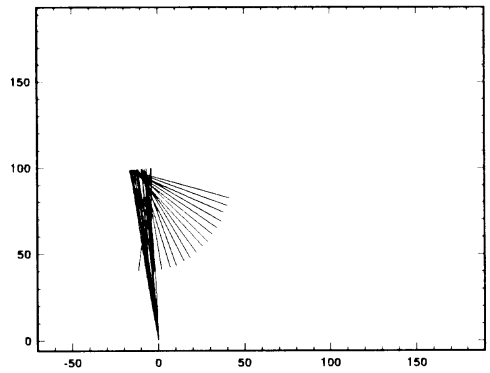

(c) 4 sec - 6 sec

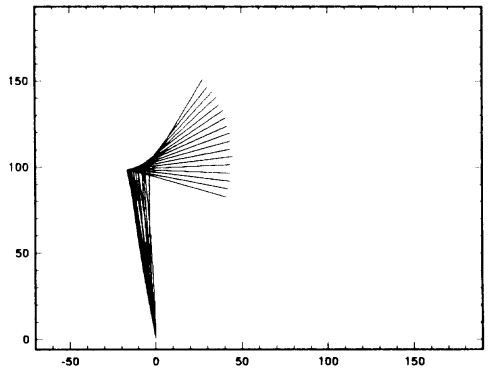

(d) 6 sec - 8 sec

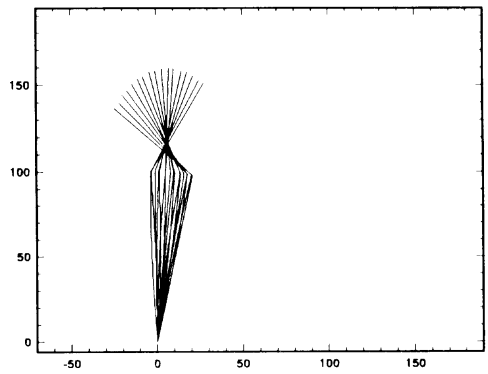

(e) 8 sec - 10 sec

Fig. 26. Time-lapse responses of a two-arm robot with open loop control (0–10 s) with time increment 0.125 s.

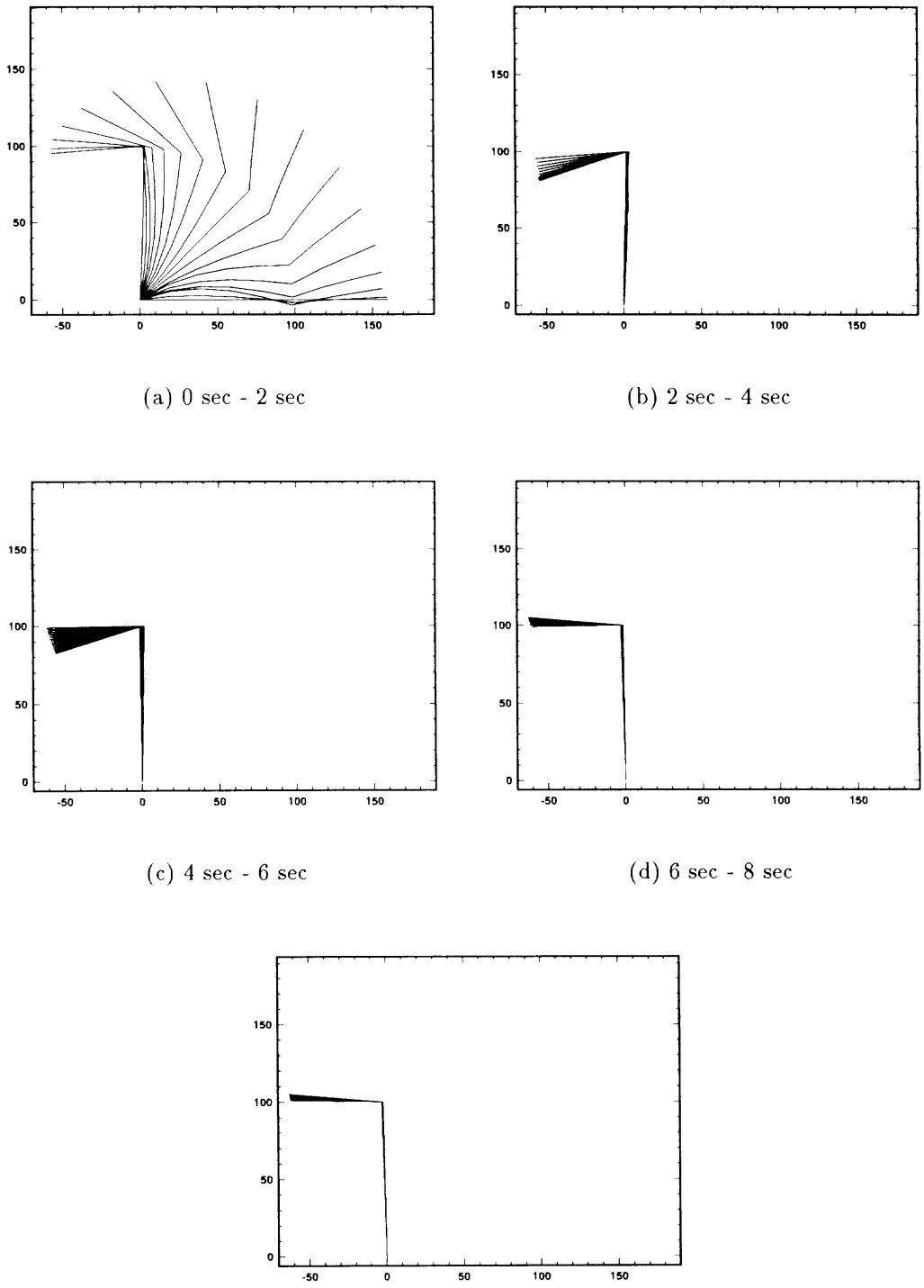

(a) 0 sec - 2 sec

(b) 2 sec - 4 sec

(c) 4 sec - 6 sec

(d) 6 sec - 8 sec

(e) 8 sec - 10 sec

Fig. 27. Time-lapse responses of a two-arm robot with optimal closed loop control (0–10 s) with time increment 0.125 s.

where I_{L1} and I_{L2} are the mass moments of inertia about the hinge point of arms 1 and 2, respectively.

The performance function is chosen as

$$P = \sum_{t=0}^{t=T_f} \mathbf{F}_c^T \mathbf{F}_c \Delta t + w\left(t \sum_{t=0}^{t=T_f} \mid E - E_D \mid \Delta t\right), \tag{20}$$

where the closed control force vector is $\mathbf{F}_c = \{M_c^{(1)}, M_c^{(7)}\}^T$ and $T_f = 10$ s. The performance function P is minimized after selecting a weighting parameter $w = 3.0 \times 10^4$ (g cm^2/s). The optimal control gains are then obtained by optimization.

Fig. 25 compares for arm 2, the open-loop and optimal closed-loop control in tip displacement error responses. The tip displacement error is defined as the difference between the actual flexible tip displacement and the equivalent rigid body tip displacement.

The open loop response is shown in Fig. 26. Under open loop control, arm 1 oscillates near the 90° angle while arm 2 is mainly 'spinning' (rigid body motion) about the hinge point after the control force is removed. With the optimal closed-loop control, the elastic vibration and rigid body motion of the two-arm robot are nearly eliminated in the finite period T_f as shown in Fig. 27.

6. Conclusions

Four numerical problems illustrated the proposed approach for controlling the motion of elastic multilink mechanisms. The slewing beam was the simplest mechanism to control. The crank-slider problem shows a control algorithm in which the open-loop torque and the closed-loop force are not located at the same position. The four-bar mechanism problem illustrates a more complicated mechanism and control algorithm. The two-bar robot problem shows the ability of the control approach to handle the internal joints control torques. The recent dissertation by Wang (1994) documents further applications. The following points summarize the paper:

1. A simple and effective method for control of nonlinear elastic multilink mechanisms was presented.
2. The control law that manipulates the motion of elastic mechanisms, consists of open loop and closed loop components. The open loop component produces the desired overall rigid body motion, while the closed loop component suppresses the elastic motion relative to the rigid body motion.
3. Both the control law and the structural dynamics are based on an inertial coordinate system. As a result, the control forces and control moments can be easily incorporated into a large displacement dynamic finite element simulation.
4. A dynamic finite element code, based on large displacement beam theory and incorporating the control law, has been developed to simulate the motion of an elastic mechanisms.
5. The method has been illustrated for the case of planar mechanisms modeled with beam elements. However, the approach applies to other element types, large strains beam theory, and to the analysis of spatial mechanisms.

References

[1] Eischen JW, Silverberg LM, Wang H. Slewing motion control of a very flexible elastic beam. ASME J Appl Mech 1992;:684–7.
[2] Silverberg LM, Foster LA. Decentralized feedback maneuver of flexible spacecraft. J Guidance Control Dynam 1990;13:258–64.
[3] Silverberg LM, Morton M. On the nature of natural control. J Vibr, Stress Reliability Des 1989;111:412–22.
[4] Simo JC, Vu-Quoc L. On the dynamics of flexible beams under large overall motions—the plane case: part 1 and part 2. J Appl Mech 1986;53:849–63.
[5] Nikravesh PE. Computer-aided analysis of mechanical systems. Prentice-Hall, 1987.
[6] Gevarter WB. Basic relations for control of flexible vehicles. AIAA J 1971;8(4):666–72.
[7] Wang H. Control and optimization of elastic multilink mechanisms. Ph.D. thesis. North Carolina State University, Department of Mechanical and Aerospace Engineering, 1994.
[8] Silverberg LM, Yunis IS. The compromise inherent in structure feedback control. Appl Math Modeling 1990;14:362–9.
[9] Dennis JE Jr, Schnabel RB. Numerical methods for unconstrained optimization and nonlinear equation. Prentice-Hall, 1983.